Available online at www.sciencedirect.com
SCIENCE DIRECT®
Planetary and Space Science 52 (2004) 679–684
Planetary and Space Science
www.elsevier.com/locate/pss

Ion cyclotron instability triggered by drifting minor ion species: Cascade effect and exact results

L. Gomberoff*, V. Muñoz, J.A. Valdivia

Departmento de Física, Facultad de Ciencias, Universidad de Chile, Casilla 653, Santiago, Chile

Received 10 July 2003; received in revised form 21 January 2004; accepted 29 January 2004

Abstract

On the basis of bi-Maxwellian velocity distribution functions it has been recently shown that the combined effect of heavy ion thermal anisotropy and drift velocity can trigger ion–cyclotron instabilities beyond the corresponding heavy ion–cyclotron frequency. (Proton–cyclotron instability induced by the thermal anisotrophy of minor ions. J. Geophys. Res. 107 (2002) 1494; Ion–cyclotron instability due to the thermal anisotrophy of drifting ion species. J. Geophys. Res. 108 (2003) 1050.) Here we show that the cascade-type mechanism proposed by Gomberoff and Valdivia (2002, 2003) can take place in the region where main heating of the fast solar wind seems to occur (i.e. within 10 solar radii). We also compare some of the results obtained by using the semi-cold approximation with the exact kinetic dispersion relation.

Keywords: Ion–cyclotron; Drifting ions; Cascade effect; Coronal holes; Solar wind; Heating; Acceleration

1. Introduction

Recent observations and theoretical results seem to indicate that most of the acceleration and heating of high-speed solar wind streams occur within a few solar radii from the Sun (Kohl et al., 1997, 1998; Cranmer et al., 1999a, b, c, d; Esser et al., 1999; Hu and Habbal, 1999; Kohl et al., 1999a, b; Cranmer, 2000, 2002). It is also widely believed that the main heating and acceleration mechanism is due to resonant absorption of ion–cyclotron waves (for a review see Isenberg, 2001; Hollweg and Isenberg, 2002; Cranmer, 2002). However, the power spectrum of magnetic fluctuations observed at distances larger than 0.3 AU shows Alfvén waves with frequencies ranging from 0.001–0.1 Hz, which are not likely to heat and accelerate the ions to the observed values. On the other hand, Alfvén waves with frequencies ranging between $10–10^4$ Hz, which are capable of heating and accelerating the heavy ions to the observed values, have not yet been observed either in the solar wind or in the solar corona (Cranmer et al., 1999a, b). However, there are a number of proposals as to how these high-frequency waves might be produced. Thus, it has been suggested that high-frequency Alfvén waves might be generated by microflares that are then converted to ion–cyclotron waves at higher coronal altitudes (Axford and McKenzie, 1992, 1996). Other suggestions involve a turbulent cascade from low-frequency Alfvén waves to high frequency ion–cyclotron waves (see, e.g., Tu and Marsch, 1995).

More recently, following the observation that heavy ions, such as O^{+5} and Mg^{+9} can reach very large thermal anisotropies close to the base of coronal holes (Esser et al., 1999; Kohl et al., 1999a), it was shown by Gomberoff and Valdivia (2002, 2003) that the thermal anisotropy of drifting heavy ion species can trigger ion–cyclotron waves above their corresponding ion-gyrofrequency. This was shown assuming bi-Maxwellian distribution functions for the ions. The problem involving two and three minor heavy ion species was fully investigated in Gomberoff and Valdivia (2002, 2003). The treatment of Gomberoff and Valdivia (2002, 2003) made use of the semi-cold approximation, which requires the argument of the dispersion functions to be much larger than one, and the assumption that the real part of the argument is much larger than the imaginary part (Gomberoff and Neira, 1983; Gomberoff and

* Corresponding author. Fax: 562-271-2973.
E-mail address: lgombero@abello.dic.uchile.cl (L. Gomberoff).

0032-0633/$ - see front matter © 2004 Elsevier Ltd. All rights reserved.
doi:10.1016/j.pss.2004.01.004

Elgueta, 1991; Gomberoff, 1992). These assumptions might put some limitation on the results that may be critical in the region where this mechanism might play a role. In Gomberoff and Valdivia (2002, 2003) the high-frequency branch of the unstable spectrum—the branch close to the proton gyrofrequency—was shown to be very rapidly stabilized with increasing parallel proton temperature. By solving the hot plasma dispersion relation we shall show that the full theory allows for parallel proton temperatures ($\beta_{\|p}$) larger than the ones predicted by the semi-cold approximation.

Another point related to these studies is the following. Gomberoff et al. (1996) argued that if only small frequency Alfvén waves are triggered at the base of coronal holes, they can only belong to the branch of the dispersion relation which starts at $\omega = 0$. As the drift velocity of the minor ions increases the branch will eventually reach the proton gyrofrequency. It was argued by Hollweg and Isenberg (2002) that the α-particle branch of the dispersion relation can reach the proton gyrofrequency for drift velocities normalized to the Alfvén velocity, of the order of 0.17, which according to Hu and Habbal (1999), may occur at distances of the order of 10 solar radii, far away from the region where main heating is taking place. Although this may be valid in a two ion-component plasma, it is not true in the presence of 3 or more ion species, or in the presence of thermal effects in the dispersion relation (Gomberoff et al., 1996; Gomberoff and Astudillo, 1999). Moreover, in Gomberoff and Valdivia (2002, 2003) it was argued that due to the fact that a drifting thermally anisotropic ion species can trigger ion–cyclotron waves above its gyrofrequency, a cascade-type mechanism capable of generating high-frequency waves starting from relatively low-frequency waves (but still much larger than those thought to be launched by the Sun with the most power) can take place. The idea is that if an ion species of low charge to mass ratio becomes thermally anisotropic and accelerated due to the resonant interaction with low frequency Alfvén waves, it can trigger ion–cyclotron waves above its gyrofrequency. In turn this can contribute to accelerate and heat anisotropically species with higher charge to mass ratio, in a process that can lead to a cascade-type mechanism capable of generating high-frequency waves starting from low frequency waves. This would be an additional mechanism to the turbulent cascade mentioned above (Tu and Marsch, 1995; Hollweg, 1999a, b).

Thus, here we do two things. (1) We solve the exact kinetic dispersion relation. We do this in order to compare the solutions with the semi-cold approximation for those cases where the difference can play an important role in the generation of high-speed solar wind streams within a few solar radii. (2) We show that the cascade-like mechanism proposed by Gomberoff and Valdivia (2002, 2003) can occur for α-particles drift velocities, normalized to the Alfvén velocity, less than 0.17. Hence, this is more consistent with regions where expected heating seems to occur (Hu and Habbal, 1999).

2. Ion–cyclotron dispersion relation

We consider a plasma in an external magnetic field B_0, composed of electrons, protons, and a number of heavy ion species drifting relative to the protons along the external magnetic field. The jth minor heavy ion species has normalized velocity $U_j = V_j/V_A$, where V_j is the heavy ion velocity and $V_A = B_0/\sqrt{4\pi n_p m_p}$ is the Alfvén velocity, with n_p the proton density and m_p the proton mass. The dispersion relation for ion–cyclotron waves moving in the direction of the external magnetic field, assuming bi-Maxwellian distribution functions, is (see, e.g., Gomberoff, 1992),

$$y^2 = \sum_j \left\{ \frac{z_j \eta_j A_j}{M_j} - z_j \eta_j (x - y U_j) - \frac{z_j \eta_j}{M_j^2 y \beta_{\|j}^{1/2}} Z(\xi_j) G_j \right\}, \quad (1)$$

$$G_j = [A_j(1 - M_j(x - y U_j)) - M_j(x - y U_j)], \quad (2)$$

where the sum is over all ion species, including the proton background. In Eq. (1), $x = \omega/\Omega_p$, $y = kV_A/\Omega_p$, $\eta_j = n_j/n_p$, $A_j = T_{\perp j}/T_{\|j} - 1$ is the ion thermal anisotropy, $M_j = m_j/z_j m_p$ (with m_j the ion mass and z_j the degree of ionization of the heavy ion), Z is the plasma dispersion function (Fried and Conte, 1961), $\xi_j = (M_j(x - yU_j) - 1)/M_j y \beta_{\|j}^{1/2}$, $\beta_{\|j} = v_{th,\|j}^2/V_A^2$, where $v_{th,\|j}^2 = 2KT_{\|j}/m_j$ is the thermal velocity of ion components, and K is the Boltzmann constant. In this equation we have assumed a current-free system, and the bulk protons has been chosen to be the rest frame (Gomberoff, 1992).

We assume now a plasma composed of electrons, isotropic protons, and O^{+6} ions. The reason for using O^{+6} instead of O^{+5}, is because the effect we want to illustrate depends on the concentration of the heavy ions, and since after protons and α-particles the O^{+6} are the most abundant, we have used O^{+6} rather than the observed O^{+5} (see also discussion in Gomberoff and Valdivia, 2002, 2003).

$$y^2 = -x + \frac{x}{y\beta_{\|p}^{1/2}} Z(\xi_p) - 6\eta_{O^{+6}}(x - yU_{O^{+6}}) + \frac{6\eta_{O^{+6}} A_{O^{+6}}}{16/6} - \frac{6\eta_{O^{+6}}}{(16/6)^2 y \beta_{\|O^{+6}}^{1/2}} Z(\xi_{O^{+6}}) \times (A_{O^{+6}}(1 - (16/6)(x - yU_{O^{+6}})) - (16/6)(x - yU_{O^{+6}})). \quad (3)$$

In Eq. (3) although the electrons are not cold, since $\Omega_e \ll \omega$, the argument of the corresponding Z-function is much larger than 1 and, therefore, they can be considered as being 'cold' (see Gomberoff and Cuperman, 1982). Also, in Eq. (3) x is complex, i.e. $x = \mathrm{Re}(x) + i\,\mathrm{Im}(x)$.

We solve this equation numerically. For a given value of y we find a particular solution and then follow this branch, for other y values, with a standard Newton root finding method. A comparison of the numerical results obtained by using

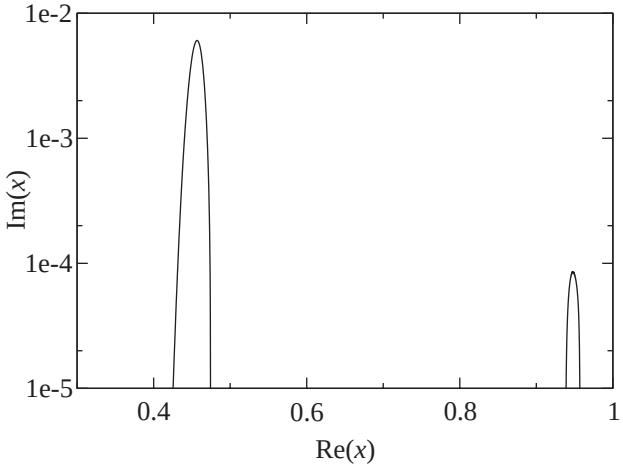

Fig. 1. Normalized growth rate $\gamma = \mathrm{Im}(x)$ vs. $\mathrm{Re}(x)$ for drifting O^{+6} ions with $U_{O^{+6}} = 0.15$, $\eta_{O^{+6}} = 2 \times 10^{-4}$, $A_{O^{+6}} = 100$, $\beta_{\|O^{+6}} = 4 \times 10^{-4}$, and $\beta_{\|p} = 10^{-5}$, obtained by using the semi-cold approximation.

Eq. (3) and the semi-cold approximation (Gomberoff and Valdivia, 2002, 2003), shows very good agreement except that the exact dispersion relation allows wave generation for larger $\beta_{\|p}$ values.

To illustrate this result, in Fig. 1 we plot the normalized growth rate $\gamma = \mathrm{Im}(\omega/\Omega_p)$ as a function of $\mathrm{Re}(x) = \mathrm{Re}(\omega/\Omega_p)$, for the case of drifting O^{+6} ions as obtained using the semi-cold approximation, for $U_{O^{+6}} = 0.15$, $\beta_{\|O^{+6}} = 4 \times 10^{-4}$, and $\beta_{\|p} = 10^{-5}$. It can be shown that the exact kinetic theory gives rise to a very similar result. Although the actual $\beta_{\|p}$ values in the region of interest is almost 2 orders of magnitude higher, we have used this example in order to show that for very small $\beta_{\|p}$ the semi-cold approximation is a very good approximation.

In Fig. 2, $\beta_{\|p}$ has been raised to $\beta_{\|p} = 2.7 \times 10^{-5}$. In Fig. 2a the result obtained from the semi-cold approximation shows that the high-frequency peak is completely stabilized, while the exact theory gives a small effect as shown in Fig. 2b. In this example, we wanted to show that the exact theory allows for larger $\beta_{\|p}$ values, although they are still very small as compared to real values.

Another difference is obtained for larger drift velocities. In this case, the growth rate of the high-frequency branch is higher and broader than the one obtained using the semi-cold approximation, as illustrated in Fig. 3. Fig. 3a shows the semi-cold approximation result for $U_{O^{+6}} = 0.18$, and Fig. 3b the corresponding exact kinetic result for $\beta_{\|p} = 10^{-5}$ (solid lines). In this case, the exact theory shows that the effect is still present for $\beta_{\|p} = 10^{-4}$ as displayed on Fig. 3b with dashed lines/circles, while in the semi-cold approximation the high-frequency region is completely stabilized.

In Fig. 4 we show the result using the exact theory for $U_{O^{+6}} = 0.23$. Solid lines correspond to the case when $\beta_{\|p} = 10^{-4}$ and dashed lines/circles to the case when $\beta_{\|p} = 10^{-3}$. Note that in the semi-cold approximation $\gamma_m < 10^{-4}$ for $\beta_{\|p} = 10^{-5}$ (see Gomberoff and Valdivia, 2002). Thus, the

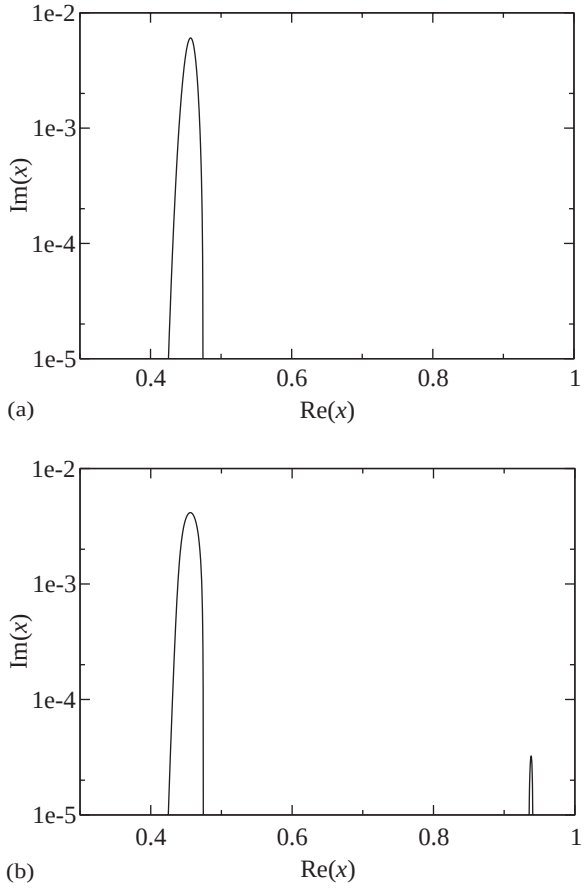

Fig. 2. Same as Fig. 1, but for $\beta_{\|p} = 2.7 \times 10^{-5}$. (a) Semi-cold approximation and (b) kinetic theory.

exact theory allows for almost two orders of magnitude increase of $\beta_{\|p}$.

Now we turn to the cascade-like phenomenon discussed by Gomberoff and Valdivia (2002, 2003). To this end, we consider three ion components: O^{+6}, α-particles, and background protons. In such case, the dispersion relation, Eq. (1) yields,

$$
\begin{aligned}
y^2 = {} & -x + \frac{x}{y\beta_{\|p}^{1/2}} Z(\xi_p) - 6\eta_{O^{+6}}(x - yU_{O^{+6}}) \\
& + \frac{6\eta_{O^{+6}} A_{O^{+6}}}{16/6} - \frac{6\eta_{O^{+6}}}{(16/6)^2 y\beta_{\|O^{+6}}^{1/2}} Z(\xi_{O^{+6}}) \\
& \times (A_{O^{+6}}(1 - (16/6)(x - yU_{O^{+6}})) \\
& - (16/6)(x - yU_{O^{+6}})) - 2\eta_\alpha(x - yU_\alpha) \\
& + \frac{2\eta_\alpha A_\alpha}{2} - \frac{2\eta_\alpha}{4y\beta_{\|\alpha}^{1/2}} Z(\xi_\alpha)(A_\alpha(1 - 2(x - yU_\alpha)) \\
& - 2(x - yU_\alpha)). \qquad (4)
\end{aligned}
$$

In Fig. 5 we plot the growth rate obtained from the semi-cold approximation for Eq. (4) (Gomberoff and Valdivia, 2003). Solid lines correspond to instabilities in

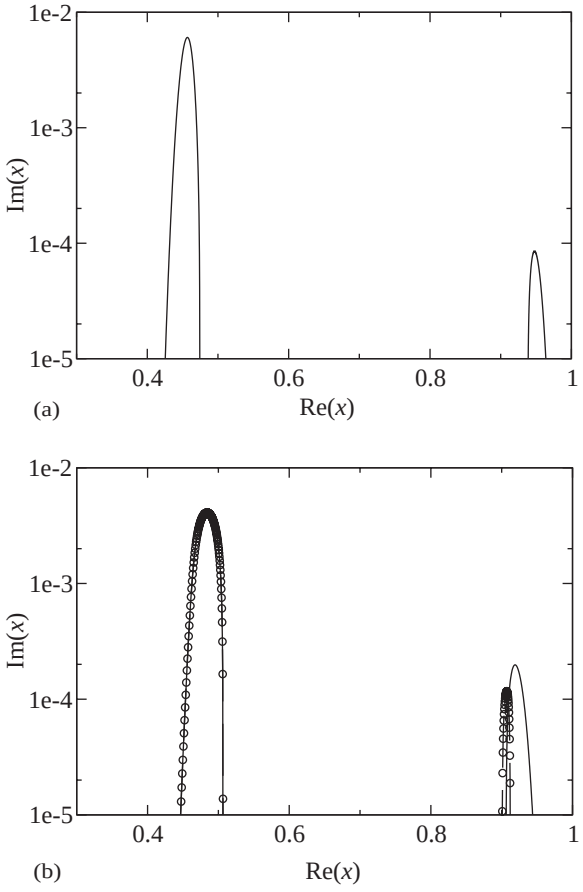

Fig. 3. Same as Fig. 1, but for $U_{O^{+6}} = 0.18$. (a) Semi-cold approximation for $\beta_{\|p} = 10^{-5}$, (b) kinetic theory (solid lines, $\beta_{\|p} = 10^{-5}$; dashed lines and circles, $\beta_{\|p} = 10^{-4}$).

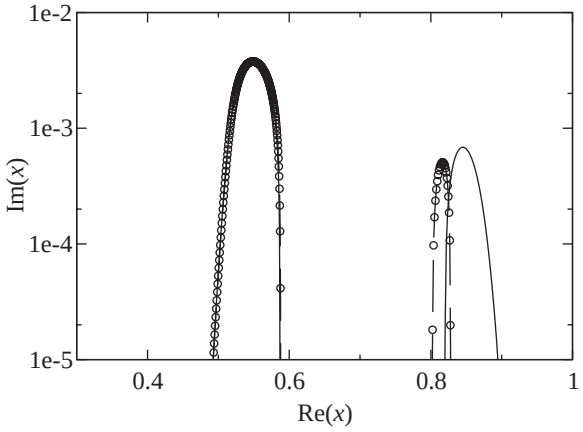

Fig. 4. Same as Fig. 1, but for $U_{O^{+6}} = 0.23$, for $\beta_{\|p} = 10^{-4}$ (solid lines), and $\beta_{\|p} = 10^{-3}$ (dashed lines and circles), using Eq. (3) in both cases.

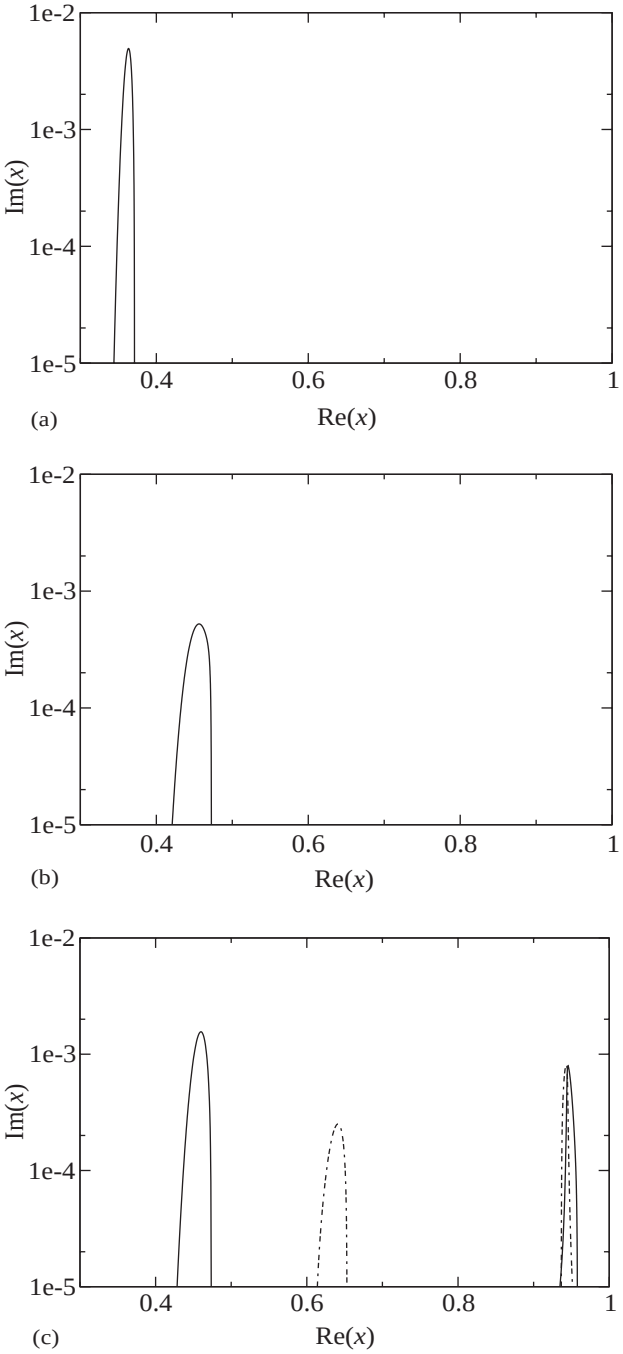

Fig. 5. Normalized growth rate $\gamma = \mathrm{Im}(x)$ vs. $\mathrm{Re}(x)$ for the semi-cold approximation for Eq. (4), using $\eta_{O^{+6}} = 2 \times 10^{-4}$, $\eta_\alpha = 0.05$, $\beta_{\|p} = 10^{-5}$, $\beta_{\|O^{+6}} = 4 \times 10^{-4}$, $\beta_{\|\alpha} = 10^{-4}$, $A_{O^{+6}} = 100$, $A_\alpha = 0$. Solid line: instabilities in the oxygen branch; dashed line: instabilities in the α-branch. (a) $U_{O^{+6}} = U_\alpha = 0$. (b) $U_{O^{+6}} = 0.12$. (c) $U_{O^{+6}} = 0.14$, $U_\alpha = 0.12$, $A_\alpha = 20$, and $A_{O^{+6}} = 50$.

the oxygen branch, and dashed lines to instabilities in the α-branch.

In Fig. 5a we illustrate the growth rate γ as a function of $\mathrm{Re}(x)$, for $\eta_{O^{+6}} = 2 \times 10^{-4}$, $\eta_\alpha = 0.05$, $\beta_{\|p} = 10^{-5}$, $\beta_{\|O^{+6}} = 4 \times 10^{-4}$, $\beta_{\|\alpha} = 10^{-4}$, $A_{O^{+6}} = 100$, $A_\alpha = 0$, and $U_{O^{+6}} = U_\alpha = 0$. As expected, the growth rate is below the O^{+6} gyrofrequency, $(\Omega_{O^{+6}}/\Omega_p) = 0.375$. As the O^{+6} drift velocity increases, the growth rate becomes broader and moves toward the α-particle gyrofrequency $(\Omega_\alpha/\Omega_p) = 0.5$. This is illustrated in Fig. 5b for $U_{O^{+6}} = 0.12$. Once the α-particles are anisotropically heated they are also accelerated. In Fig. 5c we illustrate a possible situation corresponding to $U_{O^{+6}} =$

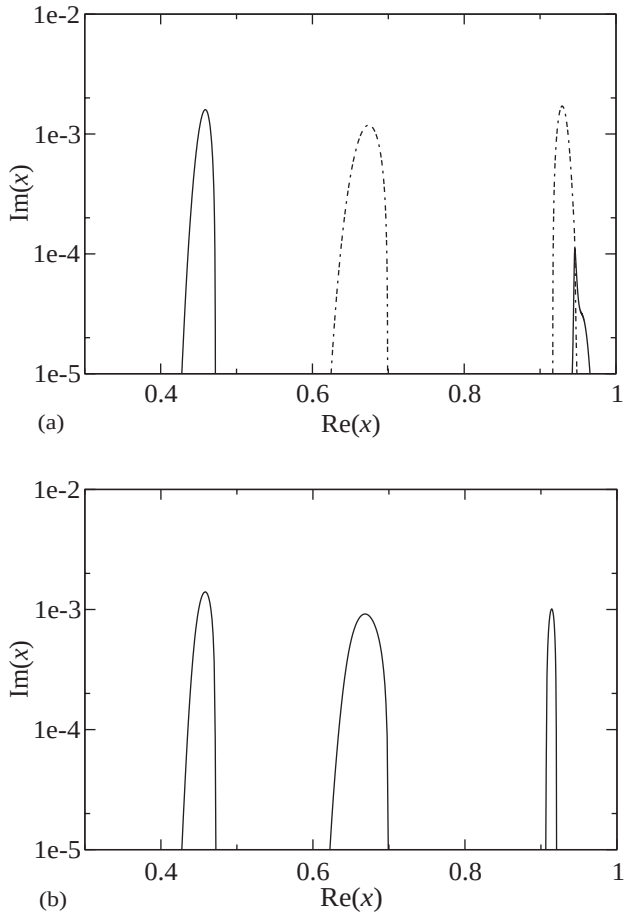

Fig. 6. Same as Fig. 5. (a) $U_\alpha = 0.13$ and $A_\alpha = 25$. The other parameters are like in Fig. 5c, using the semi-cold approximation for $\beta_{\|p} = 10^{-5}$. Solid line: instabilities in the oxygen branch; dashed line: instabilities in the α-branch. (b) $\beta_{\|p} = 10^{-4}$ obtained from the exact dispersion relation Eq. (4).

0.14, $U_\alpha = 0.12$, $A_\alpha = 20$, and $A_{O^{+6}} = 50$ with the other parameters like in Fig. 5a. We see that the growth rate below the α-particle gyrofrequency becomes larger, and two new peaks appear above the α-particle gyrofrequency. One in the region between $0.6 < \mathrm{Re}(x) < 0.7$, and the other close to the proton gyrofrequency. The one close to the proton gyrofrequency can heat up the protons. Note that in Fig. 5c we have also reduced the O^{+6} thermal anisotropy, because the oxygen has been accelerated and the α-particles have become anisotropic at the expense of the oxygen thermal anisotropy. Note also that everything occurs for $U_\alpha = 0.12$ which is less than 0.17. Therefore, this mechanism can heat the protons within 10 solar radii from the Sun (Hu and Habbal, 1999; Hollweg and Isenberg, 2002).

Finally, in Fig. 6 we have taken $U_\alpha = 0.13$ and $A_\alpha = 25$. The other parameters are like in Fig. 5c. In Fig. 6a we show the result obtained by using the semi-cold approximation for $\beta_{\|p} = 10^{-5}$. In Fig. 6b we show the same situation as in Fig. 6a, but for $\beta_{\|p} = 10^{-4}$, obtained from the exact dispersion relation Eq. (4). Note that for $\beta_{\|p} = 10^{-4}$ the kinetic dispersion relation still allows some wave activity in the high-frequency region. In the semi-cold approximation the high-frequency instability region is completely stabilized for $\beta_{\|p} = 10^{-4}$.

In conclusion, we see that the semi-cold approximation is a very good approximation except for the fact that the kinetic theory allows wave generation for larger $\beta_{\|p}$ values. These values may be more realistic than those used by Gomberoff and Valdivia (2002, 2003) in coronal holes within 10 solar radii.

3. Summary

As mentioned before in Gomberoff and Valdivia (2002, 2003), the values used for $\beta_{\|p}$ are probably too small for the base of coronal holes. These results were obtained by using the semi-cold approximation. By using the exact kinetic theory we have shown that, quite generally the agreement is very good, except for the fact that the exact theory allows for larger $\beta_{\|i}$ threshold values than the semi-cold approximation. In other words, proton-cyclotron waves can still be excited for $\beta_{\|p}$ values larger than those obtained from the semi-cold approximation. This result can be relevant close to the base of solar coronal holes where the $\beta_{\|p}$ values can be slightly larger than those used in Gomberoff and Valdivia (2002). We have also shown that the cascade-like mechanism proposed by Gomberoff and Valdivia (2002, 2003) can trigger ion–cyclotron waves close to the proton gyrofrequency for α-particle drift velocities less than 0.17, normalized to the Alfvén velocity, allowing thereby proton heating within 10 solar radii in agreement with some models (see Hu and Habbal, 1999). Since minor branching density ratios are very small, except for α-particles and O^{+6}, one might think that the present mechanism cannot be very efficient. However, as shown in Gomberoff and Valdivia (2002, 2003), the effect depends not only on the density, but also on the thermal anisotropy, relative drift speed between ion species, and ion temperatures. Nevertheless, we do not expect this effect to be the only one responsible for this phenomenon as also explained in Gomberoff and Valdivia (2002, 2003).

Finally, we want to emphasize the fact that the present model is based on the assumption of bi-Maxwellian distribution functions. In Cranmer (2001), it was shown that the instability which occurs for large bi-Maxwellian anisotropies may be strongly suppressed when the ion velocity distribution is curved along the resonant shells that grow in the presence of ion–cyclotron damping. On the other hand, it may be that other kinds of anisotropic distributions may not be as unstable as bi-Maxwellian. These aspects deserve further investigation.

Acknowledgements

This work has been partially supported by FONDECYT grants No. 1020152, No. 1030727 and No. 1020558.

References

Axford, W.I., McKenzie, J.F., 1992. The origin of the high speed solar wind streams. University Press, New York, pp. 1–5.

Axford, W.I., McKenzie, J.F., 1996. Acceleration of the solar wind. In: Winterhalter, D. et al. (Eds.), Solar Wind Eighth AIP Conference and Proceedings, pp. 382–385.

Cranmer, S.R., 2000. Ion cyclotron wave dissipation in the solar corona: the summed effect of more than 2000 ion species. Astrophys. J. 532, 1197–1208.

Cranmer, S.R., 2001. Ion cyclotron diffusion of velocity distributions in the extended solar corona. J. Geophys. Res. 106, 24,937–24,954.

Cranmer, S.R., 2002. Coronal holes and the high-speed solar wind. Space Sci. Rev. 101, 229–294.

Cranmer, S.R., Field, G.B., Kohl, J.L., 1999a. Spectroscopic constraints on models of ion-cyclotron resonance heating in the polar solar corona. Space Sci. Rev. 87, 149–152.

Cranmer, S.R., Field, G.B., Kohl, J.L., 1999b. Spectroscopic constraints on models of ion-cyclotron resonance heating in the polar solar corona and high speed solar wind. Astrophys. J. 518, 937–947.

Cranmer, S.R., Kohl, J.L., Noci, G., Antonucci, E., et al., 1999c. An empirical model of a polar coronal hole at solar minimum. Astrophys. J. 511, 481–501.

Cranmer, S.R., Field, G.B., Kohl, J.L., 1999d. The impact of ion–cyclotron wave dissipation on heating and accelerating the fast solar wind. In: Habbal, S. et al. (Eds.), Solar Wind Ninth AIP Conference Proceedings, pp. 35–39.

Esser, R., Fineschi, S., Dobrzycka, D., Habbal, S.R., et al., 1999. Plasma properties in coronal holes derived from measurements of minor ion spectral lines and polarized white light intensity. Astrophys. J. Lett. 510, L63–L67.

Fried, B.D., Conte, S.D., 1961. The Plasma Dispersion Function. Academic, San Diego, California.

Gomberoff, L., 1992. Electrostatic waves in the Earth's magnetotail and in comets, and electromagnetic instabilities in the magnetosphere and the solar wind. IEEE Trans. Plasma Sci. 20, 843–866.

Gomberoff, L., Cuperman, S., 1982. Combined effect of cold H^+ and He^+ ions on the proton cyclotron electromagnetic instability. J. Geophys. Res. 87, 95–100.

Gomberoff, L., Neira, R., 1983. Convective growth rate of ion-cyclotron waves in a $H^+ - He^+$ and $H^+ - He^+ - O^+$ plasma. J. Geophys. Res. 88, 2170–2174.

Gomberoff, L., Elgueta, R., 1991. Resonant acceleration of α-particles by ion–cyclotron waves in the solar wind. J. Geophys. Res. 96, 9801–9804.

Gomberoff, L., Gratton, F.T., Gnavi, G., 1996. Acceleration and heating of heavy ions by circularly polarized Alfvén waves. J. Geophys. Res. 101, 15661–15666.

Gomberoff, L., Astudillo, H., 1999. Ion heating and acceleration in the solar wind. In: Habbal, S. et al. (Eds.), Solar Wind Ninth AIP Conference and Proceedings, pp. 461–464.

Gomberoff, L., Valdivia, J.A., 2002. Proton–cyclotron instability induced by the thermal anisotropy of minor ions. J. Geophys. Res. 107, 1494, doi:10.1029/2002JA009357.

Gomberoff, L., Valdivia, J.A., 2003. Ion–cyclotron instability due to the thermal anisotropy of drifting ion species. J. Geophys. Res. 108, 1050, doi:10.1029/2002JA009576.

Hollweg, J.V., 1999a. Cyclotron resonance in coronal holes: 1. Heating and acceleration of protons, O^{5+}, and Mg^{9+}. J. Geophys. Res. 104, 24781–24792.

Hollweg, J.V., 1999b. Potential wells, the cyclotron resonance, and ion heating in coronal holes. J. Geophys. Res. 104, 505–520.

Hollweg, J.V., Isenberg, P.A., 2002. Generation of the fast solar wind: a review with emphasis on the resonant cyclotron interaction. J. Geophys. Res. 107, 1147, doi:10.1029/2001JA000270.

Hu, Y.Q., Habbal, S.R., 1999. Resonant acceleration and heating of solar wind by dispersive ion cyclotron waves. J. Geophys. Res. 104, 17045–17056.

Isenberg, P.A., 2001. The kinetic shell model of coronal heating and acceleration by ion cyclotron waves: 2. Inward and outward propagating waves. J. Geophys. Res. 106, 29249–29260.

Kohl, J.L., Esser, R., Cranmer, S.R., Fineschi, S., et al., 1999a. EUV spectral line profiles in polar coronal holes from 1.3 to 3.0 r. Astrophys. J. 510, L59–L62.

Kohl, J.L., Fineschi, S., Esser, R., Ciaravella, A., et al., 1999b. UVCS/SOHO observations of spectral line profiles in polar coronal holes. Space Sci. Rev. 87, 233–236.

Kohl, J.L., Noci, G., Antonucci, E., Tondello, G., et al., 1997. First results from the SOHO ultraviolet coronagraph spectrometer. Solar Phys. 175, 613–644.

Kohl, J.L., Noci, G., Antonucci, E., Tondello, G., et al., 1998. UVCS/SOHO empirical determinations of anisotropic velocity distributions in the solar corona. Astrophys. J. 501, L127–L131.

Tu, C.-Y., Marsch, E., 1995. MHD structures, waves, and turbulence in the solar wind: observations and theories. Space Sci. Rev. 73, 1–210.